Artificial Intelligence in Coronary Artery Disease

Subjects: Cardiac & Cardiovascular Systems
Contributor: Nitesh Gautam , , Mark Rabbat , Gianluca Pontone , Yiye Zhang , Benjamin Lee , Subhi AlAref

Clinically significant atherosclerosis of the coronary arteries, known as coronary artery disease (CAD), is an endemic condition that is associated with significant morbidity and mortality. The introduction of artificial intelligence (AI) and machine learning over the last two decades has unlocked new dimensions in the field of cardiovascular medicine. From automatic interpretations of heart rhythm disorders via smartwatches, to assisting in complex decision-making, AI has quickly expanded its realms in medicine and has demonstrated itself as a promising tool in helping clinicians guide treatment decisions. Understanding complex genetic interactions and developing clinical risk prediction models, advanced cardiac imaging, and improving mortality outcomes are just a few areas where AI has been applied in the domain of coronary artery disease.

artificial intelligence | coronary artery disease | major adverse cardiovascular events

1. Integration of Genetics and AI in Cardiovascular Diseases

Over the last two decades, the emergence of technologies able to measure biological processes at a large scale have resulted in an enormous influx of data. For instance, the completion of the Human Genome Project has paved the way to design single-nucleotide polymorphism (SNP) and mRNA microarrays, which can broadly test for millions of genetic variants in a simple point-of-care test. This has paved the way for the emergence of modern data-driven sciences such as genomics and other “omics” [1]. Genome-wide association studies (GWASs) operate by simultaneous comparison of millions of SNPs between diseased individuals and disease-free controls to detect a statistically significant association between an SNP locus and a particular condition [1]. Machine learning (ML) and particularly deep learning (DL) algorithms are inherently designed to extract patterns and associations from large-scale data, including clinical and genomic data. Given the complexity and multifaceted nature of cardiovascular diseases in general, and CAD in particular, an approach that integrates all these factors into a risk-stratification model would be expected to better predict incident events than existent models [2].

Multiple studies have emphasized the role of ML in identifying genetic variants and expression patterns associated with CAD from mRNA arrays using differential expression analysis and protein–protein interaction networks [3][4]. For example, Zhang et al. used ML to perform differential expression analysis on mRNA profiles from CAD patients and healthy controls to identify a set of differentially expressed genes between the two groups, then built a network representation of functional protein–protein interaction. The top 20 genes in the network were identified using a maximal clique centrality (MCC) algorithm. Finally, to test the performance, a logistic regression model was built

using the top five predictor genes to classify individuals into the presence or absence of CAD. The model achieved an AUC of 0.9295 and 0.8674 in the training and internal validation sets respectively [5].

Dogan et al. built an ensemble model of eight random-forest (RF) classifiers to predict the risk of symptomatic CAD using genetic and epigenetic variables along with clinical risk factors. The model was trained on a cohort derived from the Framingham heart study (*n* = 1545) and utilized variables derived from genome-wide array chips to extract epigenetic (DNA methylation loci) and genetic (SNP) profiles. The initial number of available variables were 876,014 SNP and DNA methylation (CpG) loci, which required multiple reduction steps, ending up with 4 CpG and 2 SNP predictors fed into the model along with age and gender. The model predicted symptomatic CAD with an accuracy, sensitivity, and specificity of 0.78, 0.75, and 0.80, respectively, in the internal validation cohort (*n* = 142).

Finally, the coronary artery calcium (CAC) score, calculated using the Agatston method on noncontrast ECG-gated cardiac computed tomography, is an established strong predictor of major adverse cardiovascular events in asymptomatic individuals. Genomic studies have previously focused on identifying genetic loci linked to CAC [6][7]. Oguz et al. suggested the use of ML algorithms to predict advanced CAC from SNP arrays and clinical variables. They identified a set of SNPs that ranked the highest in predictive importance and correlated with advanced CAC scores, defined as the 89th–99th percentile CAC scores in the derivation and replication cohorts, and trained different RF models to predict advanced CAC scores using clinical and genetic variables.

2. Risk Prediction Models and Imaging Modalities for Estimating Pretest Probability of CAD

Traditionally, stratifying patients presenting with stable chest pain using pretest probability (PTP) estimates of CAD has been commonly used to help with decision-making regarding downstream testing and the choice of an appropriate diagnostic modality. Historically, the Diamond–Forrester model—developed using age, sex, and chest pain characteristics—was used as a clinician's risk stratification tool in predicting the PTP of CAD [8]. However, numerous studies showed its limitation in overestimating PTP by approximately threefold, especially in women [9]. This led to the development of the updated Diamond–Forrester model (UDF) and the CAD consortium score [10][11][12]. These scores, incorporating demographic and clinical risk factors, have been proven to be better at predicting the risk of CAD. Therefore, improving the ability to predict CAD using more accurate risk-assessment modeling is imperative, given the potential to reduce downstream testing and associated costs. Using clinical and demographic features, ML models have been employed to estimate the PTP of CAD [13][14][15]. In a recent multicenter cross-sectional study, a deep neural network algorithm based on the facial profile of individuals was able to achieve a higher performance than traditional risk scores in predicting PTP of CAD (AUC for the ML model 0.730 vs. 0.623 for Diamond –Forrester and 0.652 for the CAD consortium, $p < 0.001$) [16]. Though the study is limited by the lack of external validity and low specificity (54%), such approaches can potentially lead to a paradigm change in CAD management by facilitating earlier detection and initiation of primary prevention using readily available parameters, such as an individual's facial profile.

When available, a CAC score has been shown to add to the PTP of CAD, with a CAC score of zero identifying low-risk patients who might not need additional testing [17][18]. ML models, combining clinical and imaging parameters, have been shown to have higher predictive power than traditional risk scores when predicting the PTP of obstructive CAD [19][20].

Various ML algorithms based on stress imaging, particularly single-photon emission computed tomography (SPECT), have been devised to facilitate the prediction of CAD. These models combined the clinical and demographic characteristics with the quantitative variables, as evaluated via SPECT to better predict CAD compared with the visual interpretation or quantitative variables alone [21][22][23][24][25][26].

Cardiac phase-space analysis is a novel noninvasive diagnostic platform that combines advanced disciplines of mathematics and physics with ML [27]. Thoracic orthogonal voltage gradient (OVG) signals from a patient are evaluated by cardiac phase-space analysis to quantify physiological and mathematical features associated with CAD. The analysis is performed at the point of care without the need for a change in physiologic status or radiation. Initial multicenter results suggest that resting cardiac phase-space analysis may have comparable diagnostic utility to functional tests currently used to assess CAD [28].

Finally, the assessment of regional wall motion abnormalities (RWMAs) on echocardiography has been associated with the presence of obstructive CAD, and as such can be useful in helping clinicians with downstream decision-making [29].

3. Artificial Intelligence in Management of CAD in the Emergency Department

Chest pain is a common emergency department presentation, and distinguishing cardiac from noncardiac pain causes is crucial for optimal management. Modalities such as electrocardiography (ECG) serve as a quick way to recognize patterns associated with unstable CAD, and in particular acute coronary syndromes (ACSs). Deep neural networks have shown a consistent performance in image recognition, and models have hence been devised to identify patterns related to CAD and myocardial infarction (MI) [30][31][32]. By reducing interobserver variability and providing accurate results efficiently, this approach holds the promise of improving workflow across healthcare systems, while helping patients in areas of limited medical infrastructure and specialized care.

The 2021 American College of Cardiology/American Heart Association (ACC/AHA) chest pain guidelines advocate for the use of coronary CT angiography (CCTA) in intermediate-risk patients presenting with acute chest pain who either have no known history or a history of nonobstructive CAD (defined as coronary artery disease with less than 50% diameter stenosis) [18]. Given the ability of CCTA to accurately define coronary anatomy and extent/distribution of atherosclerotic plaque, it has been consistently shown to be a useful noninvasive imaging modality for patient selection, particularly for those who might require further invasive evaluation. However, interpretation of CCTA scans requires expertise and is time-intensive. Therefore, automatic interpretation of CCTA, which can lead to a significant reduction in the processing times, is highly desirable. ML algorithms have recently been developed,

achieving a 70–75% reduction in reading time compared to that required for human interpretation (2.3 min for AI vs. 7.6–9.6 min for human readers). Though the model described performed slightly lower than highly experienced readers in interpreting CCTA (AUC 0.93 vs. 0.90 for human vs. AI, $p < 0.05$), when combined with low-experience human readers, it augmented the reader's ability to correctly reclassify obstructive CAD (per-vessel net reclassification index (NRI) 0.07, $p < 0.001$) [33]. In addition, ML has been applied for various segmentation and classification tasks on cardiac CT imaging, from automatic segmentation of calcified and noncalcified plaque to automated calculation of the Agatston CAC score, and finally quantification of cardiac structures on CT imaging (**Figure 1**) [34][35][36][37][38][39][40][41]. Therefore, the application of ML could provide reliable results in real time, while bridging the dearth of experts in low-resource settings.

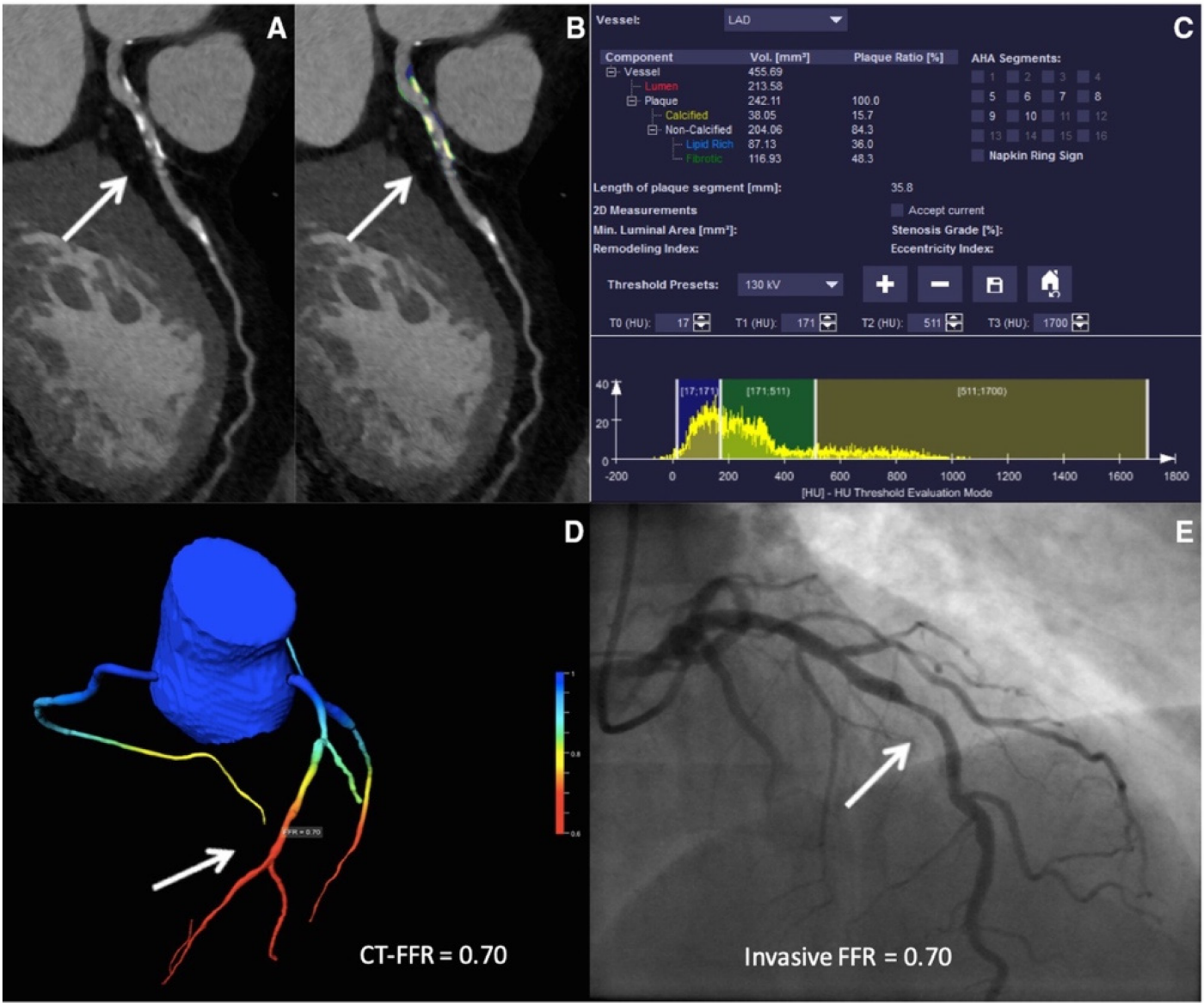

Figure 1. ML-based fractional flow reserve from cardiac CT ($CT\text{-}FFR_{ML}$). Machine-learning-based coronary plaque analysis quantifies atherosclerotic plaque into calcified and noncalcified components (**A**,**B**). This is further integrated with other quantitative parameters (**C**) and transformed into 3-D images of the vessels to give $CT\text{-}FFR_{ML}$

(**D**), which has been shown to have a good correlation with invasive fractional flow reserve (FFR—**E**). Adapted with permission from Von Knebel Doeberitz et al. [33], Elsevier.

Stress testing, which provides an estimate of myocardial perfusion and viability, has been recommended as an alternative to CCTA in intermediate-risk chest pain patients [18]. Myocardial perfusion imaging, particularly SPECT, has been employed to recognize patients who might need an invasive evaluation, with a diagnostic sensitivity of 75–88% and specificity of 60–79% [42][43][44][45][46][47]. SPECT can be evaluated qualitatively in terms of size, severity, location, and reversibility of perfusion defect, and quantitatively, in terms of total perfusion deficit (TPD), summed stress score (SSS), summed rest score (SRS), as well as stress and rest volumes [48]. Automatically generated polar maps (representing radiotracer distribution in a two-dimensional plane) after three-dimensional segmentation of the left ventricle (LV) have been used as raw data for quantitative analysis. After the LV polar map is divided into 17 segments, each of the segments is graded on a scale of 0–4 based on the severity of ischemia. The scores are then summated to generate SSS and SRS [49]. Polar maps also provide information about the overall extent and magnitude of ischemia, in terms of TPD [49][50]. These objective variables extracted from the quantitative analysis offer an increased degree of reproducibility and can be incorporated into risk scores to predict mortality [50][51]. The diagnostic accuracy of qualitative and quantitative approaches is comparable, as has been shown in numerous studies [52]. A deep convolutional neural network-based model derived from polar maps (**Figure 2**) had a superior performance compared to TPD in predicting obstructive coronary artery disease (the AUC for ML were 0.80 and 0.76 vs. 0.78 and 0.73 for TPD on a per-patient and per-vessel basis respectively, $p < 0.01$). In addition to diagnosis, models to predict early revascularization (<90 days from SPECT) have been developed and have demonstrated better performance than individual SPECT variables on a per-patient and a per-vessel level [53][54].

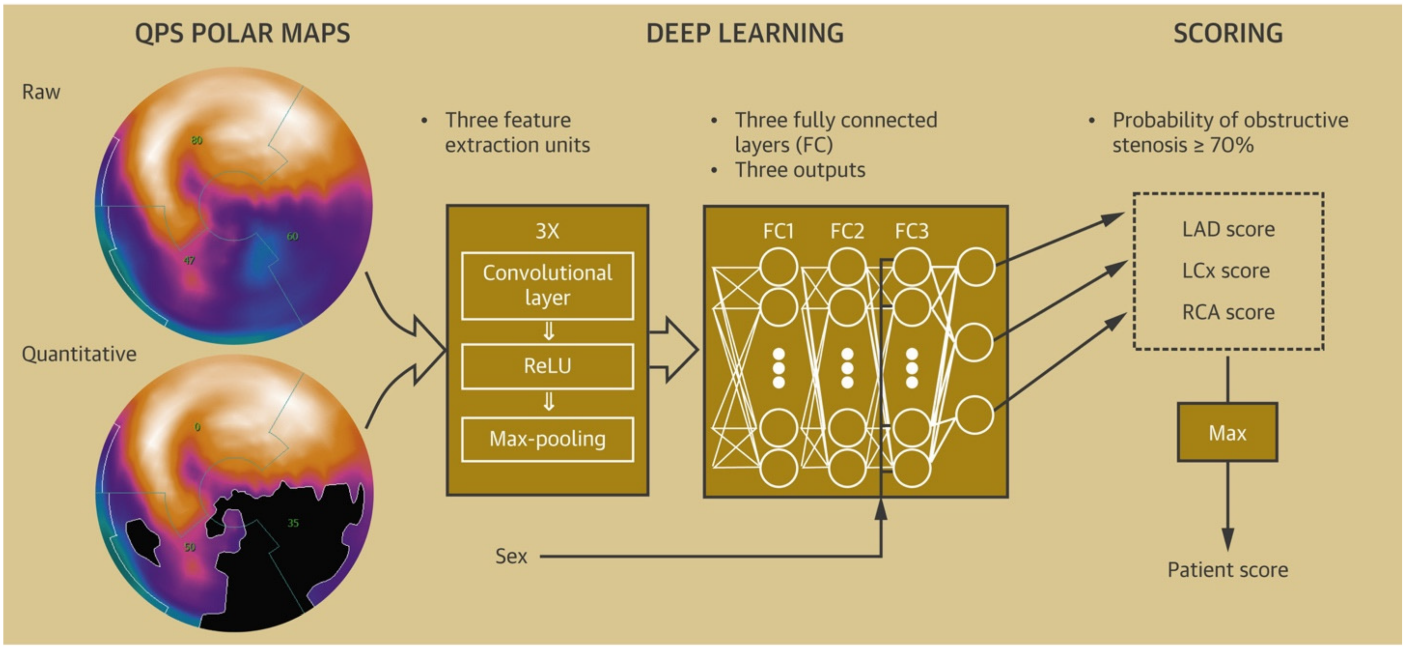

Figure 2. Deep-learning model to predict obstructive CAD from polar maps. Raw polar maps and extent polar maps (maps with abnormal pixels representing ischemia blackened out) are fed into deep neural networks, with the

extracted data used to calculate scores for individual vessels to predict the probability of CAD. Adapted with permission from Betancur et al. [25], Elsevier.

4. Artificial Intelligence to Predict Functionally Obstructive CAD and Lesion-Specific Ischemia—As a Gatekeeper to the Catheterization Laboratory

4.1. ML-Based CT-FFR Estimation and Diagnostic Accuracy

Based on the concept of artery lumen segmentation, the ML-based FFR estimation (CT-FFR_{ML}) has generated significant interest in the past few years. The CT-FFR_{ML} model was trained on 12,000 synthetically generated coronary geometric datasets and used deep neural networks, allowing for automatic computation of FFR in real-time [55]. Coenen et al. performed a multicenter, prospective study to evaluate the diagnostic performance of CT-FFR_{ML} to predict lesion-specific ischemia, comparing it with traditional CCTA parameters, with invasive FFR being the gold standard [56]. They demonstrated an excellent correlation between CT-FFR_{ML} and FFR_{CT} (r = 0.997) and a superior performance of CT-FFR_{ML} over traditional CCTA in predicting lesion-specific ischemia (AUC: 0.84 vs. 0.69, $p < 0.001$ on a per-vessel level). Since then, multiple retrospective studies have been performed to evaluate the diagnostic accuracy of CT-FFR_{ML}, validated against the gold-standard invasive FFR. They have further demonstrated superior diagnostic performance of CT-FFR_{ML} over CTA stenosis severity and quantitative atherosclerotic plaque features derived from CCTA [38][55][56][57][58][59][60][61][62][63][64][65][66].

4.2. Impact of Calcification Burden on the Performance of CT-FFR_{ML}

The impact of coronary calcification on the diagnostic performance of CCTA has been well-established, with more extensive calcification limiting the ability of CCTA to evaluate for the presence of obstructive CAD [67][68][69]. Multiple indices have been devised to compute a CAC score, with the Agatston score, calcium volume, calcification remodeling index (CRI), and segmental arc calcification method being common examples [70]. The Agatston Score (AS) is the most widely validated approach, which summates the calcium score (function of peak density and area of the lesion) of the individual lesions across all coronary artery segments [71]. CRI provides a lesion-specific calcium estimate and is calculated as a ratio of the cross-sectional luminal area of the most severely calcified site to the proximal luminal area [72]. The segmental arc calcification method estimates lesion-specific calcium burden by measuring the greatest circumferential extent of coronary calcium, grading as nil (noncalcified), mild (0–90°), moderate (90–180°), and severe (>180°) calcification [69][73].

4.3. CT-FFR_{ML} in Predicting Revascularization Events

CT-FFR_{ML} has been shown to be a better predictor than plaque features derived from CCTA for the determination of the presence of lesion-specific ischemia, but whether CT-FFR_{ML} influences the eventual treatment plan and outcomes (as guided by ICA-FFR) remains an active area of investigation [74][75][76][77]. Qiao et al. demonstrated the added benefit of CT-FFR_{ML} compared to relying on an anatomy-based strategy in patients with stable chest

pain (reduction rate of ICA by 54.5% and 4.4% fewer revascularizations) [74]. Additionally, adding CT-FFR_{ML} to CCTA can decrease the rate of unnecessary ICA by 35.2% (thereby increasing the proportion of revascularizations when ICA is undertaken), truly acting as a gatekeeper to ICA. Furthermore, lower CT-FFR_{ML} was associated with higher major adverse cardiovascular event (MACE) risk when compared to diameter stenosis on CCTA (HR, 6.84 vs. 1.47) or ICA (HR, 6.84 vs. 1.84). Liu et al. found a similar rate of MACE (2.9%) after revascularization based on either combining CCTA stenosis ≥ 50% and CT-FFR_{ML} ≤ 0.8 or ICA stenosis ≥ 75% in a 2-year follow-up [75]. It further highlighted the use of CT-FFR_{ML} as a gatekeeper to ICA with a positive impact on lower healthcare costs.

CT-FFR_{ML} comes with its own set of shortcomings. The diagnostic performance of the CT-FFR_{ML} model is lower, with the invasive FFR closely approaching the diagnostic threshold of 0.8 [56][58][78]. Traditional statistical and DL approaches have shown that stenosis severity; plaque characteristics, such as low-density, noncalcified plaque; and remodeling index are independent predictors of lesion-specific ischemia that are not related to CT-FFR_{ML} [79][80]. An integrated DL approach in the future that combines clinical features, anatomical plaque characteristics, vessel features, and functional assessment could potentially overcome this limitation.

5. Artificial Intelligence in the Field of Intracoronary Imaging

5.1. Artificial Intelligence to Optimize Peri-Intervention Workflow

To predict OCT-derived TCFA on IVUS images, Bae et al. created a ML model, enrolling 517 patients who underwent ICA [81]. A total of 40,908 IVUS-OCT co-registered sections in 517 coronary arteries were divided into training and testing sets in a ratio of 4:1. An artificial-neural-network-based model using 17 features achieved the highest performance with a sensitivity and specificity of 85 ± 4% and 79 ± 6%, respectively, and good discriminatory power (AUC of 0.80 ± 0.08). Larger plaque burden, minimal diameter, decreased lumen area, and increased lumen eccentricity were seen to be strongly associated with OCT-derived TCFAs. Min et al. utilized a deep learning algorithm (densely connected convolutional neural network) on 35,678 OCT frames to automatically detect TCFAs from OCT images [82]. After the frames were interpreted for the presence/absence of TCFA, data was fed into the algorithm to devise a deep-learning model. By achieving high sensitivity and specificity of 88.7 ± 3.4% and 91.8 ± 2.0% on the test data, such deep-learning models can significantly reduce processing times and allow for easy interpretation when it comes to identifying a vulnerable high-risk plaque.

5.2. Applications of Artificial Intelligence in Intra and Post-Intervention Workflow

Optimal stent expansion is vital to successful outcomes, with stent underexpansion predisposing to stent restenosis and a greater stent expansion exposing the procedure to a risk of stent edge dissection [83]. IVUS, by allowing direct visualization of vessel architecture, can help in the earlier identification and management of these complications. Nishi et al. developed a ML model to compute the luminal area and the vessel area accurately, as well as the stent area, which exhibited an excellent correlation between ML-derived and expert-derived dimensions while dramatically reducing the time required for segmentation of IVUS images (37 s) compared with expert analysis (30 h) [84].

Virtual histology IVUS (VH-IVUS) is a well-studied intracoronary imaging modality used for in vivo visualization of high-risk plaques [85][86][87][88]. Zhang et al. devised a deep-learning model to predict the location of high-risk plaques in nonculprit vessels in patients who underwent IVUS at baseline and after one year [89].

6. Artificial Intelligence-Based Post-Procedure Risk Prediction Models

In addition to early detection and the institution of guideline-directed therapy in the appropriate risk strata, accurate prediction of unheralded adverse events forms the cornerstone for managing CAD. Identifying the high-risk target population can potentially provide a window for aggressive risk factor modulation, thereby reducing mortality and contributing towards better health at a population level. Multiple risk-prediction models have been developed to predict in-hospital mortality and the long-term risk of MACE in high-risk cohorts [90][91][92][93][94][95][96][97].

PCI is a relatively safe procedure, with a reported overall in-hospital mortality rate of 1–2% [98]. The risk of complications increases with increasing patient morbidity, with an incidence of technical difficulties and periprocedural complications 2.2 times higher than in the average population [99]. The Mayo clinic risk score (MCRS) and New York State risk score (NYSRS) were developed to predict in-hospital and 30-day mortality in patients undergoing PCI. Both scores performed equivalently well, showing an excellent discriminative ability to identify patients at a higher risk for in-hospital and 30-day mortality [100]. They employed regression-based models, assuming a linear interplay between patient variables and mortality outcomes. ML models have been recently developed to potentially uncover complex and nonlinear relationships between multiple factors, hence improving diagnostic accuracy over current models.

7. Artificial Intelligence-Based Long-Term Mortality and MACE Prediction Models

Prognostic modeling via ML has been validated with the use of electronic health records (EHRs) integrated with clinical scores and imaging modalities to predict MACE [101][102][103]. Utilizing the array of data available in EMR and identifying patterns based on clinical course, ML models have been used to create a personalized treatment algorithm (ML4CAD) for every patient, based on risk factors, past medical history, time present in the EMR system, and medications. The illustrated model makes clinical decisions for patients based on these factors and suggests a decision with an aim to increase prescription effectiveness, evaluated in the terms of time from initial diagnosis to the first potential adverse event (time to adverse event, TAE). The model had superior performance when compared to standard of care, increasing the time to adverse event (TAE) from 4.56 to 5.66 years (24.3% increase), hence furthering the idea of precision medicine [102][104].

Multiple ML techniques have been proposed to automatically evaluate CAC score from dedicated cardiac and non-EKG gated chest CT scans [34][35][105][106][107]. ML techniques incorporating CAC score and other imaging parameters have been shown to be a better predictor than the traditional risk scores employed for cardiovascular

disease risk stratification [108][109][110][111][112]. An ensemble-boosting model developed by Nakanishi et al. incorporating a total of 77 clinical and imaging variables had a superior discriminatory power for predicting coronary heart disease deaths than imaging and clinical data alone (AUC for ML model: 0.845 compared to 0.821 and 0.781 for clinical data and CAC respectively, $p < 0.001$) (**Figure 3**) [113].

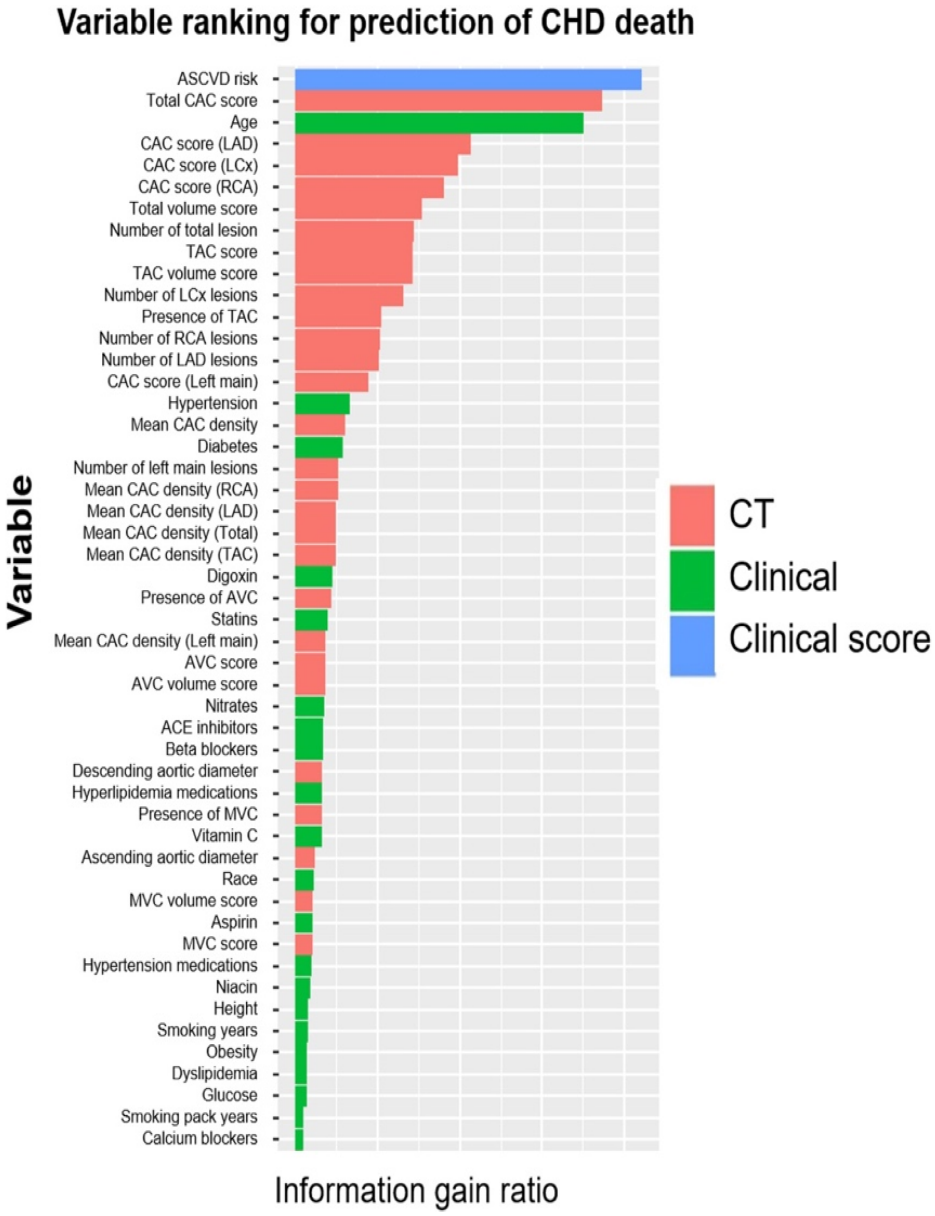

Figure 3. Variable importance as determined by the ML model for prediction of coronary heart disease deaths. Abbreviations: CAC: coronary artery calcium; TAC: thoracic aortic calcification; AVC: aortic valve calcification; MVC: mitral valve calcifications; LAD: left anterior descending; LCx: left circumflex RCA: right coronary artery. Adapted with permission from Nakanishi et al. [113], Elsevier.

Apart from CAC scoring and traditional CT metrics, the role of EAT volume and attenuation in the prediction of future cardiovascular risk has been an active area of research. Deep-learning approaches to automatically compute EAT volume and EAT attenuation from CT have been developed, significantly reducing generation time from 15 min to 2 s [109].

Although anatomical CT scores and plaque features provide useful diagnostic and prognostic data, the complex interplay of factors at the molecular level, in addition to patient-level characteristics leading to specific phenotypic manifestations in terms of plaque burden and features, is not well-elucidated and remains an area of active research. In particular, elucidating important factors that “drive” the process of atherosclerotic plaque formation and progression is not only vital from a therapeutic perspective, but it can also improve risk-assessment strategies. Recent studies have demonstrated that coronary artery inflammation inhibits lipid accumulation in the perivascular adipose tissue [114]. This results in a higher attenuation of the affected perivascular area, identified on CCTA as the fat attenuation index (FAI). FAI has been shown to be a sensitive marker of coronary inflammation, with higher FAI values (≥−70.1 HU) independently predicting cardiovascular mortality [114][115]. A posthoc analysis of the CRISP-CT study showed an incremental value of adding FAI to high-risk plaque characteristics, pointing towards a more significant role of these precursor lesions in predicting patient outcomes [116]. A more recent ML approach created a pericoronary fat ‘radiomic’ profile (FRP), identifying radiomic variables predicting tissue inflammation, fibrosis, and vascularity on CCTA [117]. The incorporation of FRP significantly improved the MACE predictive ability of the traditional model (AUC for traditional + FRP 0.88 vs. 0.754 for the traditional model, $p < 0.001$). Using a cut-off of 0.63, individuals in the high FRP group were at a higher risk of MACE (HR = 10.84, $p < 0.001$). Importantly, Kaplan–Meir analysis showed an additional value of FRP over high-risk plaque (HRP) characteristics in predicting long-term survival (HR for the FRP-/HRP+ subgroup 5.97, $p = 0.03$ compared to 43.33 for the FRP+/HRP+ subgroup). Such ‘radiotranscriptomic’ approaches incorporating molecular biology and radiology and evaluating their interaction via artificial intelligence can help uncover deeper relationships between metabolic pathways and clinical outcomes, helping to better understand the pathophysiology and elements involved in the clinical progression of cardiovascular disease.

References

1. Sprangers, M.A.G.; Sloan, J.A.; Barsevick, A.; Chauhan, C.; Dueck, A.C.; Raat, H.; Shi, Q.; Van Noorden, C.J.F.; Consortium, G. Scientific imperatives, clinical implications, and theoretical underpinnings for the investigation of the relationship between genetic variables and patient-reported quality-of-life outcomes. Qual. Life Res. 2010, 19, 1395–1403.
2. Eraslan, G.; Avsec, Ž.; Gagneur, J.; Theis, F.J. Deep learning: New computational modelling techniques for genomics. Nat. Rev. Genet. 2019, 20, 389–403.
3. Wang, Y.; Liu, T.; Liu, Y.; Chen, J.; Xin, B.; Wu, M.; Cui, W. Coronary artery disease associated specific modules and feature genes revealed by integrative methods of WGCNA, MetaDE and machine learning. Gene 2019, 710, 122–130.
4. Balashanmugam, M.V.; Shivanandappa, T.B.; Nagarethinam, S.; Vastrad, B.; Vastrad, C. Analysis of Differentially Expressed Genes in Coronary Artery Disease by Integrated Microarray Analysis. Biomolecules 2019, 10, 35.

5. Zhang, D.; Guan, L.; Li, X. Bioinformatics analysis identifies potential diagnostic signatures for coronary artery disease. J. Int. Med. Res. 2020, 48, 300060520979856.
6. Ferguson, J.F.; Matthews, G.J.; Townsend, R.R.; Raj, D.S.; Kanetsky, P.A.; Budoff, M.; Fischer, M.J.; Rosas, S.E.; Kanthety, R.; Rahman, M.; et al. Candidate gene association study of coronary artery calcification in chronic kidney disease: Findings from the CRIC study (Chronic Renal Insufficiency Cohort). J. Am. Coll. Cardiol. 2013, 62, 789–798.
7. O'Donnell, C.J.; Kavousi, M.; Smith, A.V.; Kardia, S.L.; Feitosa, M.F.; Hwang, S.J.; Sun, Y.V.; Province, M.A.; Aspelund, T.; Dehghan, A.; et al. Genome-wide association study for coronary artery calcification with follow-up in myocardial infarction. Circulation 2011, 124, 2855–2864.
8. Diamond, G.A.; Forrester, J.S. Analysis of probability as an aid in the clinical diagnosis of coronary-artery disease. N. Engl. J. Med. 1979, 300, 1350–1358.
9. Foldyna, B.; Udelson, J.E.; Karády, J.; Banerji, D.; Lu, M.T.; Mayrhofer, T.; Bittner, D.O.; Meyersohn, N.M.; Emami, H.; Genders, T.S.S.; et al. Pretest probability for patients with suspected obstructive coronary artery disease: Re-evaluating Diamond-Forrester for the contemporary era and clinical implications: Insights from the PROMISE trial. Eur. Heart J. Cardiovasc. Imaging 2019, 20, 574–581.
10. Genders, T.S.; Steyerberg, E.W.; Alkadhi, H.; Leschka, S.; Desbiolles, L.; Nieman, K.; Galema, T.W.; Meijboom, W.B.; Mollet, N.R.; de Feyter, P.J.; et al. A clinical prediction rule for the diagnosis of coronary artery disease: Validation, updating, and extension. Eur. Heart J. 2011, 32, 1316–1330.
11. Genders, T.S.; Steyerberg, E.W.; Hunink, M.G.; Nieman, K.; Galema, T.W.; Mollet, N.R.; de Feyter, P.J.; Krestin, G.P.; Alkadhi, H.; Leschka, S.; et al. Prediction model to estimate presence of coronary artery disease: Retrospective pooled analysis of existing cohorts. BMJ 2012, 344, e3485.
12. Bittencourt, M.S.; Hulten, E.; Polonsky, T.S.; Hoffman, U.; Nasir, K.; Abbara, S.; Di Carli, M.; Blankstein, R. European Society of Cardiology-Recommended Coronary Artery Disease Consortium Pretest Probability Scores More Accurately Predict Obstructive Coronary Disease and Cardiovascular Events Than the Diamond and Forrester Score: The Partners Registry. Circulation 2016, 134, 201–211.
13. Li, D.; Xiong, G.; Zeng, H.; Zhou, Q.; Jiang, J.; Guo, X. Machine learning-aided risk stratification system for the prediction of coronary artery disease. Int. J. Cardiol. 2021, 326, 30–34.
14. Velusamy, D.; Ramasamy, K. Ensemble of heterogeneous classifiers for diagnosis and prediction of coronary artery disease with reduced feature subset. Comput. Methods Programs Biomed. 2021, 198, 105770.

15. Muhammad, L.J.; Al-Shourbaji, I.; Haruna, A.A.; Mohammed, I.A.; Ahmad, A.; Jibrin, M.B. Machine Learning Predictive Models for Coronary Artery Disease. SN Comput. Sci. 2021, 2, 350.
16. Lin, S.; Li, Z.; Fu, B.; Chen, S.; Li, X.; Wang, Y.; Wang, X.; Lv, B.; Xu, B.; Song, X.; et al. Feasibility of using deep learning to detect coronary artery disease based on facial photo. Eur. Heart J. 2020, 41, 4400–4411.
17. Budoff, M.J.; Mayrhofer, T.; Ferencik, M.; Bittner, D.; Lee, K.L.; Lu, M.T.; Coles, A.; Jang, J.; Krishnam, M.; Douglas, P.S.; et al. Prognostic Value of Coronary Artery Calcium in the PROMISE Study (Prospective Multicenter Imaging Study for Evaluation of Chest Pain). Circulation 2017, 136, 1993–2005.
18. Gulati, M.; Levy, P.D.; Mukherjee, D.; Amsterdam, E.; Bhatt, D.L.; Birtcher, K.K.; Blankstein, R.; Boyd, J.; Bullock-Palmer, R.P.; Conejo, T.; et al. 2021 AHA/ACC/ASE/CHEST/SAEM/SCCT/SCMR Guideline for the Evaluation and Diagnosis of Chest Pain: A Report of the American College of Cardiology/American Heart Association Joint Committee on Clinical Practice Guidelines. Circulation 2021, 78, e187–e285.
19. Baskaran, L.; Ying, X.; Xu, Z.; Al'Aref, S.J.; Lee, B.C.; Lee, S.E.; Danad, I.; Park, H.B.; Bathina, R.; Baggiano, A.; et al. Machine learning insight into the role of imaging and clinical variables for the prediction of obstructive coronary artery disease and revascularization: An exploratory analysis of the CONSERVE study. PLoS ONE 2020, 15, e0233791.
20. Al'Aref, S.J.; Maliakal, G.; Singh, G.; van Rosendael, A.R.; Ma, X.; Xu, Z.; Alawamlh, O.A.H.; Lee, B.; Pandey, M.; Achenbach, S.; et al. Machine learning of clinical variables and coronary artery calcium scoring for the prediction of obstructive coronary artery disease on coronary computed tomography angiography: Analysis from the CONFIRM registry. Eur. Heart J. 2020, 41, 359–367.
21. Arsanjani, R.; Xu, Y.; Dey, D.; Fish, M.; Dorbala, S.; Hayes, S.; Berman, D.; Germano, G.; Slomka, P. Improved accuracy of myocardial perfusion SPECT for the detection of coronary artery disease using a support vector machine algorithm. J. Nucl. Med. 2013, 54, 549–555.
22. Betancur, J.; Hu, L.H.; Commandeur, F.; Sharir, T.; Einstein, A.J.; Fish, M.B.; Ruddy, T.D.; Kaufmann, P.A.; Sinusas, A.J.; Miller, E.J.; et al. Deep Learning Analysis of Upright-Supine High-Efficiency SPECT Myocardial Perfusion Imaging for Prediction of Obstructive Coronary Artery Disease: A Multicenter Study. J. Nucl. Med. 2019, 60, 664–670.
23. Guner, L.A.; Karabacak, N.I.; Akdemir, O.U.; Karagoz, P.S.; Kocaman, S.A.; Cengel, A.; Unlu, M. An open-source framework of neural networks for diagnosis of coronary artery disease from myocardial perfusion SPECT. J. Nucl. Cardiol. 2010, 17, 405–413.
24. Rahmani, R.; Niazi, P.; Naseri, M.; Neishabouri, M.; Farzanefar, S.; Eftekhari, M.; Derakhshan, F.; Mollazadeh, R.; Meysami, A.; Abbasi, M. Improved diagnostic accuracy for myocardial perfusion imaging using artificial neural networks on different input variables including clinical and quantification data. Rev. Esp. Med. Nucl. E Imagen. Mol. 2019, 38, 275–279.

25. Betancur, J.; Commandeur, F.; Motlagh, M.; Sharir, T.; Einstein, A.J.; Bokhari, S.; Fish, M.B.; Ruddy, T.D.; Kaufmann, P.; Sinusas, A.J.; et al. Deep Learning for Prediction of Obstructive Disease From Fast Myocardial Perfusion SPECT: A Multicenter Study. JACC Cardiovasc. Imaging 2018, 11, 1654–1663.
26. Arsanjani, R.; Xu, Y.; Dey, D.; Vahistha, V.; Shalev, A.; Nakanishi, R.; Hayes, S.; Fish, M.; Berman, D.; Germano, G.; et al. Improved accuracy of myocardial perfusion SPECT for detection of coronary artery disease by machine learning in a large population. J. Nucl. Cardiol. 2013, 20, 553–562.
27. Rabbat, M.G.; Ramchandani, S.; Sanders, W.E., Jr. Cardiac Phase Space Analysis: Assessing Coronary Artery Disease Utilizing Artificial Intelligence. Biomed. Res. Int. 2021, 2021, 6637039.
28. Stuckey, T.D.; Gammon, R.S.; Goswami, R.; Depta, J.P.; Steuter, J.A.; Meine, F.J., 3rd; Roberts, M.C.; Singh, N.; Ramchandani, S.; Burton, T.; et al. Cardiac Phase Space Tomography: A novel method of assessing coronary artery disease utilizing machine learning. PLoS ONE 2018, 13, e0198603.
29. Medina, R.; Panidis, I.P.; Morganroth, J.; Kotler, M.N.; Mintz, G.S. The value of echocardiographic regional wall motion abnormalities in detecting coronary artery disease in patients with or without a dilated left ventricle. Am. Heart J. 1985, 109, 799–803.
30. Acharya, U.R.; Fujita, H.; Sudarshan, V.K.; Oh, S.L.; Adam, M.; Koh, J.E.W.; Tan, J.H.; Ghista, D.N.; Martis, R.J.; Chua, C.K.; et al. Automated detection and localization of myocardial infarction using electrocardiogram: A comparative study of different leads. Knowl.-Based Syst. 2016, 99, 146–156.
31. Han, C.; Shi, L. ML–ResNet: A novel network to detect and locate myocardial infarction using 12 leads ECG. Comput. Methods Programs Biomed. 2020, 185, 105138.
32. Lih, O.S.; Jahmunah, V.; San, T.R.; Ciaccio, E.J.; Yamakawa, T.; Tanabe, M.; Kobayashi, M.; Faust, O.; Acharya, U.R. Comprehensive electrocardiographic diagnosis based on deep learning. Artif. Intell. Med. 2020, 103, 101789.
33. Liu, C.Y.; Tang, C.X.; Zhang, X.L.; Chen, S.; Xie, Y.; Zhang, X.Y.; Qiao, H.Y.; Zhou, C.S.; Xu, P.P.; Lu, M.J.; et al. Deep learning powered coronary CT angiography for detecting obstructive coronary artery disease: The effect of reader experience, calcification and image quality. Eur. J. Radiol. 2021, 142, 109835.
34. Lee, J.-G.; Kim, H.; Kang, H.; Koo, H.J.; Kang, J.-W.; Kim, Y.-H.; Yang, D.H. Fully Automatic Coronary Calcium Score Software Empowered by Artificial Intelligence Technology: Validation Study Using Three CT Cohorts. Korean J. Radiol. 2021, 22, 1764–1776.
35. van Velzen, S.G.M.; Lessmann, N.; Velthuis, B.K.; Bank, I.E.M.; van den Bongard, D.; Leiner, T.; de Jong, P.A.; Veldhuis, W.B.; Correa, A.; Terry, J.G.; et al. Deep Learning for Automatic Calcium

Scoring in CT: Validation Using Multiple Cardiac CT and Chest CT Protocols. Radiology 2020, 295, 66–79.

36. Baskaran, L.; Maliakal, G.; Al'Aref, S.J.; Singh, G.; Xu, Z.; Michalak, K.; Dolan, K.; Gianni, U.; van Rosendael, A.; van den Hoogen, I.; et al. Identification and Quantification of Cardiovascular Structures From CCTA: An End-to-End, Rapid, Pixel-Wise, Deep-Learning Method. JACC Cardiovasc. Imaging 2020, 13, 1163–1171.
37. Wang, W.; Wang, H.; Chen, Q.; Zhou, Z.; Wang, R.; Wang, H.; Zhang, N.; Chen, Y.; Sun, Z.; Xu, L. Coronary artery calcium score quantification using a deep-learning algorithm. Clin. Radiol. 2020, 75, 237.e11–237.e16.
38. von Knebel Doeberitz, P.L.; De Cecco, C.N.; Schoepf, U.J.; Duguay, T.M.; Albrecht, M.H.; van Assen, M.; Bauer, M.J.; Savage, R.H.; Pannell, J.T.; De Santis, D.; et al. Coronary CT angiography-derived plaque quantification with artificial intelligence CT fractional flow reserve for the identification of lesion-specific ischemia. Eur. Radiol. 2019, 29, 2378–2387.
39. Koo, H.J.; Lee, J.G.; Ko, J.Y.; Lee, G.; Kang, J.W.; Kim, Y.H.; Yang, D.H. Automated Segmentation of Left Ventricular Myocardium on Cardiac Computed Tomography Using Deep Learning. Korean J. Radiol. 2020, 21, 660–669.
40. Morris, E.D.; Ghanem, A.I.; Dong, M.; Pantelic, M.V.; Walker, E.M.; Glide-Hurst, C.K. Cardiac substructure segmentation with deep learning for improved cardiac sparing. Med. Phys. 2020, 47, 576–586.
41. Muscogiuri, G.; Chiesa, M.; Trotta, M.; Gatti, M.; Palmisano, V.; Dell'Aversana, S.; Baessato, F.; Cavaliere, A.; Cicala, G.; Loffreno, A.; et al. Performance of a deep learning algorithm for the evaluation of CAD-RADS classification with CCTA. Atherosclerosis 2020, 294, 25–32.
42. Fihn, S.D.; Gardin, J.M.; Abrams, J.; Berra, K.; Blankenship, J.C.; Dallas, A.P.; Douglas, P.S.; Foody, J.M.; Gerber, T.C.; Hinderliter, A.L.; et al. 2012 ACCF/AHA/ACP/AATS/PCNA/SCAI/STS Guideline for the Diagnosis and Management of Patients With Stable Ischemic Heart Disease. Circulation 2012, 126, e354–e471.
43. Biagini, E.; Shaw, L.J.; Poldermans, D.; Schinkel, A.F.; Rizzello, V.; Elhendy, A.; Rapezzi, C.; Bax, J.J. Accuracy of non-invasive techniques for diagnosis of coronary artery disease and prediction of cardiac events in patients with left bundle branch block: A meta-analysis. Eur. J. Nucl. Med. Mol. Imaging 2006, 33, 1442–1451.
44. Mahajan, N.; Polavaram, L.; Vankayala, H.; Ference, B.; Wang, Y.; Ager, J.; Kovach, J.; Afonso, L. Diagnostic accuracy of myocardial perfusion imaging and stress echocardiography for the diagnosis of left main and triple vessel coronary artery disease: A comparative meta-analysis. Heart 2010, 96, 956–966.

45. Jaarsma, C.; Leiner, T.; Bekkers Sebastiaan, C.; Crijns Harry, J.; Wildberger Joachim, E.; Nagel, E.; Nelemans Patricia, J.; Schalla, S. Diagnostic Performance of Noninvasive Myocardial Perfusion Imaging Using Single-Photon Emission Computed Tomography, Cardiac Magnetic Resonance, and Positron Emission Tomography Imaging for the Detection of Obstructive Coronary Artery Disease. J. Am. Coll. Cardiol. 2012, 59, 1719–1728.
46. Takx, R.A.P.; Blomberg, B.A.; Aidi, H.E.; Habets, J.; de Jong, P.A.; Nagel, E.; Hoffmann, U.; Leiner, T. Diagnostic Accuracy of Stress Myocardial Perfusion Imaging Compared to Invasive Coronary Angiography With Fractional Flow Reserve Meta-Analysis. Circ. Cardiovasc. Imaging 2015, 8, e002666.
47. Fleischmann, K.E.; Hunink, M.G.; Kuntz, K.M.; Douglas, P.S. Exercise echocardiography or exercise SPECT imaging? A meta-analysis of diagnostic test performance. JAMA 1998, 280, 913–920.
48. Holder, L.; Lewis, S.; Abrames, E.; Wolin, E.A. Review of SPECT myocardial perfusion imaging. J. Am. Osteopath. Coll. Radiol. 2016, 5, 5–13.
49. Czaja, M.; Wygoda, Z.; Duszańska, A.; Szczerba, D.; Głowacki, J.; Gąsior, M.; Wasilewski, J.P. Interpreting myocardial perfusion scintigraphy using single-photon emission computed tomography. Part 1. Kardiochir. Torakochirurgia Pol. 2017, 14, 192–199.
50. Slomka, P.; Xu, Y.; Berman, D.; Germano, G. Quantitative analysis of perfusion studies: Strengths and pitfalls. J. Nucl. Cardiol. Off. Publ. Am. Soc. Nucl. Cardiol. 2012, 19, 338–346.
51. Hachamovitch, R.; Hayes, S.W.; Friedman, J.D.; Cohen, I.; Berman, D.S. A prognostic score for prediction of cardiac mortality risk after adenosine stress myocardial perfusion scintigraphy. J. Am. Coll. Cardiol. 2005, 45, 722–729.
52. Arsanjani, R.; Xu, Y.; Hayes, S.W.; Fish, M.; Lemley, M., Jr.; Gerlach, J.; Dorbala, S.; Berman, D.S.; Germano, G.; Slomka, P. Comparison of fully automated computer analysis and visual scoring for detection of coronary artery disease from myocardial perfusion SPECT in a large population. J. Nucl. Med. 2013, 54, 221–228.
53. Hu, L.H.; Betancur, J.; Sharir, T.; Einstein, A.J.; Bokhari, S.; Fish, M.B.; Ruddy, T.D.; Kaufmann, P.A.; Sinusas, A.J.; Miller, E.J.; et al. Machine learning predicts per-vessel early coronary revascularization after fast myocardial perfusion SPECT: Results from multicentre REFINE SPECT registry. Eur. Heart J. Cardiovasc. Imaging 2020, 21, 549–559.
54. Arsanjani, R.; Dey, D.; Khachatryan, T.; Shalev, A.; Hayes, S.W.; Fish, M.; Nakanishi, R.; Germano, G.; Berman, D.S.; Slomka, P. Prediction of revascularization after myocardial perfusion SPECT by machine learning in a large population. J. Nucl. Cardiol. 2015, 22, 877–884.
55. Itu, L.; Rapaka, S.; Passerini, T.; Georgescu, B.; Schwemmer, C.; Schoebinger, M.; Flohr, T.; Sharma, P.; Comaniciu, D. A machine-learning approach for computation of fractional flow reserve

from coronary computed tomography. J. Appl. Physiol. 2016, 121, 42–52.

56. Coenen, A.; Kim, Y.H.; Kruk, M.; Tesche, C.; De Geer, J.; Kurata, A.; Lubbers, M.L.; Daemen, J.; Itu, L.; Rapaka, S.; et al. Diagnostic Accuracy of a Machine-Learning Approach to Coronary Computed Tomographic Angiography-Based Fractional Flow Reserve: Result From the MACHINE Consortium. Circ. Cardiovasc. Imaging 2018, 11, e007217.
57. Di Jiang, M.; Zhang, X.L.; Liu, H.; Tang, C.X.; Li, J.H.; Wang, Y.N.; Xu, P.P.; Zhou, C.S.; Zhou, F.; Lu, M.J.; et al. The effect of coronary calcification on diagnostic performance of machine learning-based CT-FFR: A Chinese multicenter study. Eur. Radiol. 2021, 31, 1482–1493.
58. Koo, H.J.; Kang, J.W.; Kang, S.J.; Kweon, J.; Lee, J.G.; Ahn, J.M.; Park, D.W.; Lee, S.W.; Lee, C.W.; Park, S.W.; et al. Impact of coronary calcium score and lesion characteristics on the diagnostic performance of machine-learning-based computed tomography-derived fractional flow reserve. Eur. Heart J. Cardiovasc. Imaging 2021, 22, 998–1006.
59. Kumamaru, K.K.; Fujimoto, S.; Otsuka, Y.; Kawasaki, T.; Kawaguchi, Y.; Kato, E.; Takamura, K.; Aoshima, C.; Kamo, Y.; Kogure, Y.; et al. Diagnostic accuracy of 3D deep-learning-based fully automated estimation of patient-level minimum fractional flow reserve from coronary computed tomography angiography. Eur. Heart J. Cardiovasc. Imaging 2020, 21, 437–445.
60. Kurata, A.; Fukuyama, N.; Hirai, K.; Kawaguchi, N.; Tanabe, Y.; Okayama, H.; Shigemi, S.; Watanabe, K.; Uetani, T.; Ikeda, S.; et al. On-Site Computed Tomography-Derived Fractional Flow Reserve Using a Machine-Learning Algorithm—Clinical Effectiveness in a Retrospective Multicenter Cohort. Circ. J. 2019, 83, 1563–1571.
61. Rother, J.; Moshage, M.; Dey, D.; Schwemmer, C.; Trobs, M.; Blachutzik, F.; Achenbach, S.; Schlundt, C.; Marwan, M. Comparison of invasively measured FFR with FFR derived from coronary CT angiography for detection of lesion-specific ischemia: Results from a PC-based prototype algorithm. J. Cardiovasc. Comput. Tomogr. 2018, 12, 101–107.
62. Tang, C.X.; Wang, Y.N.; Zhou, F.; Schoepf, U.J.; Assen, M.V.; Stroud, R.E.; Li, J.H.; Zhang, X.L.; Lu, M.J.; Zhou, C.S.; et al. Diagnostic performance of fractional flow reserve derived from coronary CT angiography for detection of lesion-specific ischemia: A multi-center study and meta-analysis. Eur. J. Radiol. 2019, 116, 90–97.
63. Tesche, C.; Otani, K.; De Cecco, C.N.; Coenen, A.; De Geer, J.; Kruk, M.; Kim, Y.H.; Albrecht, M.H.; Baumann, S.; Renker, M.; et al. Influence of Coronary Calcium on Diagnostic Performance of Machine Learning CT-FFR: Results From MACHINE Registry. JACC Cardiovasc. Imaging 2020, 13, 760–770.
64. Wang, Z.Q.; Zhou, Y.J.; Zhao, Y.X.; Shi, D.M.; Liu, Y.Y.; Liu, W.; Liu, X.L.; Li, Y.P. Diagnostic accuracy of a deep learning approach to calculate FFR from coronary CT angiography. J. Geriatr. Cardiol. 2019, 16, 42–48.

65. Wardziak, L.; Kruk, M.; Pleban, W.; Demkow, M.; Ruzyllo, W.; Dzielinska, Z.; Kepka, C. Coronary CTA enhanced with CTA based FFR analysis provides higher diagnostic value than invasive coronary angiography in patients with intermediate coronary stenosis. J. Cardiovasc. Comput. Tomogr. 2019, 13, 62–67.

66. Tesche, C.; De Cecco, C.N.; Baumann, S.; Renker, M.; McLaurin, T.W.; Duguay, T.M.; Bayer, R.R., 2nd; Steinberg, D.H.; Grant, K.L.; Canstein, C.; et al. Coronary CT Angiography-derived Fractional Flow Reserve: Machine Learning Algorithm versus Computational Fluid Dynamics Modeling. Radiology 2018, 288, 64–72.

67. Arbab-Zadeh, A.; Miller, J.M.; Rochitte, C.E.; Dewey, M.; Niinuma, H.; Gottlieb, I.; Paul, N.; Clouse, M.E.; Shapiro, E.P.; Hoe, J.; et al. Diagnostic accuracy of computed tomography coronary angiography according to pre-test probability of coronary artery disease and severity of coronary arterial calcification. The CORE-64 (Coronary Artery Evaluation Using 64-Row Multidetector Computed Tomography Angiography) International Multicenter Study. J. Am. Coll. Cardiol. 2012, 59, 379–387.

68. Chen, C.-C.; Chen, C.-C.; Hsieh, I.C.; Liu, Y.-C.; Liu, C.-Y.; Chan, T.; Wen, M.-S.; Wan, Y.-L. The effect of calcium score on the diagnostic accuracy of coronary computed tomography angiography. Int. J. Cardiovasc. Imaging 2011, 27, 37–42.

69. Vavere, A.L.; Arbab-Zadeh, A.; Rochitte, C.E.; Dewey, M.; Niinuma, H.; Gottlieb, I.; Clouse, M.E.; Bush, D.E.; Hoe, J.W.M.; de Roos, A.; et al. Coronary artery stenoses: Accuracy of 64-detector row CT angiography in segments with mild, moderate, or severe calcification--a subanalysis of the CORE-64 trial. Radiology 2011, 261, 100–108.

70. Arjmand Shabestari, A. Coronary artery calcium score: A review. Iran Red. Crescent. Med. J. 2013, 15, e16616.

71. Agatston, A.S.; Janowitz, W.R.; Hildner, F.J.; Zusmer, N.R.; Viamonte, M., Jr.; Detrano, R. Quantification of coronary artery calcium using ultrafast computed tomography. J. Am. Coll. Cardiol. 1990, 15, 827–832.

72. Yu, M.; Li, Y.; Li, W.; Lu, Z.; Wei, M.; Zhang, J. Calcification remodeling index assessed by cardiac CT predicts severe coronary stenosis in lesions with moderate to severe calcification. J. Cardiovasc. Comput. Tomogr. 2018, 12, 42–49.

73. Sekimoto, T.; Akutsu, Y.; Hamazaki, Y.; Sakai, K.; Kosaki, R.; Yokota, H.; Tsujita, H.; Tsukamoto, S.; Kaneko, K.; Sakurai, M.; et al. Regional calcified plaque score evaluated by multidetector computed tomography for predicting the addition of rotational atherectomy during percutaneous coronary intervention. J. Cardiovasc. Comput. Tomogr. 2016, 10, 221–228.

74. Qiao, H.Y.; Tang, C.X.; Schoepf, U.J.; Tesche, C.; Bayer, R.R., 2nd; Giovagnoli, D.A.; Todd Hudson, H., Jr.; Zhou, C.S.; Yan, J.; Lu, M.J.; et al. Impact of machine learning-based coronary

computed tomography angiography fractional flow reserve on treatment decisions and clinical outcomes in patients with suspected coronary artery disease. Eur. Radiol. 2020, 30, 5841–5851.

75. Liu, X.; Mo, X.; Zhang, H.; Yang, G.; Shi, C.; Hau, W.K. A 2-year investigation of the impact of the computed tomography-derived fractional flow reserve calculated using a deep learning algorithm on routine decision-making for coronary artery disease management. Eur. Radiol. 2021, 31, 7039–7046.
76. Martin, S.S.; Mastrodicasa, D.; van Assen, M.; De Cecco, C.N.; Bayer, R.R.; Tesche, C.; Varga-Szemes, A.; Fischer, A.M.; Jacobs, B.E.; Sahbaee, P.; et al. Value of Machine Learning-based Coronary CT Fractional Flow Reserve Applied to Triple-Rule-Out CT Angiography in Acute Chest Pain. Radiol. Cardiothorac. Imaging 2020, 2, e190137.
77. Nous, F.M.A.; Budde, R.P.J.; Lubbers, M.M.; Yamasaki, Y.; Kardys, I.; Bruning, T.A.; Akkerhuis, J.M.; Kofflard, M.J.M.; Kietselaer, B.; Galema, T.W.; et al. Impact of machine-learning CT-derived fractional flow reserve for the diagnosis and management of coronary artery disease in the randomized CRESCENT trials. Eur. Radiol. 2020, 30, 3692–3701.
78. Cook, C.M.; Petraco, R.; Shun-Shin, M.J.; Ahmad, Y.; Nijjer, S.; Al-Lamee, R.; Kikuta, Y.; Shiono, Y.; Mayet, J.; Francis, D.P.; et al. Diagnostic Accuracy of Computed Tomography–Derived Fractional Flow Reserve: A Systematic Review. JAMA Cardiol. 2017, 2, 803–810.
79. Gaur, S.; Ovrehus, K.A.; Dey, D.; Leipsic, J.; Botker, H.E.; Jensen, J.M.; Narula, J.; Ahmadi, A.; Achenbach, S.; Ko, B.S.; et al. Coronary plaque quantification and fractional flow reserve by coronary computed tomography angiography identify ischaemia-causing lesions. Eur. Heart J. 2016, 37, 1220–1227.
80. Kawasaki, T.; Kidoh, M.; Kido, T.; Sueta, D.; Fujimoto, S.; Kumamaru, K.K.; Uetani, T.; Tanabe, Y.; Ueda, T.; Sakabe, D.; et al. Evaluation of Significant Coronary Artery Disease Based on CT Fractional Flow Reserve and Plaque Characteristics Using Random Forest Analysis in Machine Learning. Acad. Radiol. 2020, 27, 1700–1708.
81. Bae, Y.; Kang, S.J.; Kim, G.; Lee, J.G.; Min, H.S.; Cho, H.; Kang, D.Y.; Lee, P.H.; Ahn, J.M.; Park, D.W.; et al. Prediction of coronary thin-cap fibroatheroma by intravascular ultrasound-based machine learning. Atherosclerosis 2019, 288, 168–174.
82. Min, H.S.; Yoo, J.H.; Kang, S.J.; Lee, J.G.; Cho, H.; Lee, P.H.; Ahn, J.M.; Park, D.W.; Lee, S.W.; Kim, Y.H.; et al. Detection of optical coherence tomography-defined thin-cap fibroatheroma in the coronary artery using deep learning. EuroIntervention 2020, 16, 404–412.
83. Maehara, A.; Matsumura, M.; Ali, Z.A.; Mintz, G.S.; Stone, G.W. IVUS-Guided Versus OCT-Guided Coronary Stent Implantation: A Critical Appraisal. JACC Cardiovasc. Imaging 2017, 10, 1487–1503.

84. Nishi, T.; Yamashita, R.; Imura, S.; Tateishi, K.; Kitahara, H.; Kobayashi, Y.; Yock, P.G.; Fitzgerald, P.J.; Honda, Y. Deep learning-based intravascular ultrasound segmentation for the assessment of coronary artery disease. Int. J. Cardiol. 2021, 333, 55–59.
85. Brown, A.J.; Teng, Z.; Calvert, P.A.; Rajani, N.K.; Hennessy, O.; Nerlekar, N.; Obaid, D.R.; Costopoulos, C.; Huang, Y.; Hoole, S.P.; et al. Plaque Structural Stress Estimations Improve Prediction of Future Major Adverse Cardiovascular Events After Intracoronary Imaging. Circ. Cardiovasc. Imaging 2016, 9, e004172.
86. Xie, Z.; Dong, N.; Sun, R.; Liu, X.; Gu, X.; Sun, Y.; Du, H.; Dai, J.; Liu, Y.; Hou, J.; et al. Relation between baseline plaque features and subsequent coronary artery remodeling determined by optical coherence tomography and intravascular ultrasound. Oncotarget 2017, 8, 4234–4244.
87. Stone, P.H.; Saito, S.; Takahashi, S.; Makita, Y.; Nakamura, S.; Kawasaki, T.; Takahashi, A.; Katsuki, T.; Nakamura, S.; Namiki, A.; et al. Prediction of progression of coronary artery disease and clinical outcomes using vascular profiling of endothelial shear stress and arterial plaque characteristics: The PREDICTION Study. Circulation 2012, 126, 172–181.
88. Calvert, P.A.; Obaid, D.R.; O'Sullivan, M.; Shapiro, L.M.; McNab, D.; Densem, C.G.; Schofield, P.M.; Braganza, D.; Clarke, S.C.; Ray, K.K.; et al. Association between IVUS findings and adverse outcomes in patients with coronary artery disease: The VIVA (VH-IVUS in Vulnerable Atherosclerosis) Study. JACC Cardiovasc. Imaging 2011, 4, 894–901.
89. Zhang, L.; Wahle, A.; Chen, Z.; Lopez, J.J.; Kovarnik, T.; Sonka, M. Predicting Locations of High-Risk Plaques in Coronary Arteries in Patients Receiving Statin Therapy. IEEE Trans. Med. Imaging 2018, 37, 151–161.
90. Farooq, V.; Brugaletta, S.; Serruys, P.W. The SYNTAX score and SYNTAX-based clinical risk scores. Semin Thorac Cardiovasc Surg 2011, 23, 99–105.
91. Singh, M.; Rihal, C.S.; Lennon, R.J.; Spertus, J.; Rumsfeld, J.S.; Holmes, D.R., Jr. Bedside estimation of risk from percutaneous coronary intervention: The new Mayo Clinic risk scores. Mayo Clin. Proc. 2007, 82, 701–708.
92. Chowdhary, S.; Ivanov, J.; Mackie, K.; Seidelin, P.H.; Dzavík, V. The Toronto score for in-hospital mortality after percutaneous coronary interventions. Am. Heart J. 2009, 157, 156–163.
93. Hannan, E.L.; Farrell, L.S.; Walford, G.; Jacobs, A.K.; Berger, P.B.; Holmes, D.R., Jr.; Stamato, N.J.; Sharma, S.; King, S.B., 3rd. The New York State risk score for predicting in-hospital/30-day mortality following percutaneous coronary intervention. JACC Cardiovasc. Interv. 2013, 6, 614–622.
94. MacKenzie, T.A.; Malenka, D.J.; Olmstead, E.M.; Piper, W.D.; Langner, C.; Ross, C.S.; O'Connor, G.T. Prediction of survival after coronary revascularization: Modeling short-term, mid-term, and long-term survival. Ann. Thorac. Surg. 2009, 87, 463–472.

95. O'Connor, G.T.; Malenka, D.J.; Quinton, H.; Robb, J.F.; Kellett, M.A., Jr.; Shubrooks, S.; Bradley, W.A.; Hearne, M.J.; Watkins, M.W.; Wennberg, D.E.; et al. Multivariate prediction of in-hospital mortality after percutaneous coronary interventions in 1994-1996. Northern New England Cardiovascular Disease Study Group. J. Am. Coll. Cardiol. 1999, 34, 681–691.
96. Rihal, C.S.; Grill, D.E.; Bell, M.R.; Berger, P.B.; Garratt, K.N.; Holmes, D.R., Jr. Prediction of death after percutaneous coronary interventional procedures. Am. Heart J. 2000, 139, 1032–1038.
97. Wu, C.; Hannan, E.L.; Walford, G.; Ambrose, J.A.; Holmes, D.R., Jr.; King, S.B., 3rd; Clark, L.T.; Katz, S.; Sharma, S.; Jones, R.H. A risk score to predict in-hospital mortality for percutaneous coronary interventions. J. Am. Coll. Cardiol. 2006, 47, 654–660.
98. Fanaroff, A.C.; Zakroysky, P.; Dai, D.; Wojdyla, D.; Sherwood, M.W.; Roe, M.T.; Wang, T.Y.; Peterson, E.D.; Gurm, H.S.; Cohen, M.G.; et al. Outcomes of PCI in Relation to Procedural Characteristics and Operator Volumes in the United States. J. Am. Coll. Cardiol. 2017, 69, 2913–2924.
99. Iverson, A.; Stanberry, L.I.; Tajti, P.; Garberich, R.; Antos, A.; Burke, M.N.; Chavez, I.; Gössl, M.; Henry, T.D.; Lips, D.; et al. Prevalence, Trends, and Outcomes of Higher-Risk Percutaneous Coronary Interventions Among Patients without Acute Coronary Syndromes. Cardiovasc. Revasc. Med. 2019, 20, 289–292.
100. Singh, M.; Lennon, R.J.; Gulati, R.; Holmes, D.R. Risk scores for 30-day mortality after percutaneous coronary intervention: New insights into causes and risk of death. Mayo Clin. Proc. 2014, 89, 631–637.
101. Steele, A.J.; Denaxas, S.C.; Shah, A.D.; Hemingway, H.; Luscombe, N.M. Machine learning models in electronic health records can outperform conventional survival models for predicting patient mortality in coronary artery disease. PLoS ONE 2018, 13, e0202344.
102. Bertsimas, D.; Orfanoudaki, A.; Weiner, R.B. Personalized treatment for coronary artery disease patients: A machine learning approach. Health Care Manag. Sci. 2020, 23, 482–506.
103. Farhadian, M.; Dehdar Karsidani, S.; Mozayanimonfared, A.; Mahjub, H. Risk factors associated with major adverse cardiac and cerebrovascular events following percutaneous coronary intervention: A 10-year follow-up comparing random survival forest and Cox proportional-hazards model. BMC Cardiovasc. Disord. 2021, 21, 38.
104. Krittanawong, C.; Zhang, H.; Wang, Z.; Aydar, M.; Kitai, T. Artificial Intelligence in Precision Cardiovascular Medicine. J. Am. Coll. Cardiol. 2017, 69, 2657–2664.
105. Chao, H.; Shan, H.; Homayounieh, F.; Singh, R.; Khera, R.D.; Guo, H.; Su, T.; Wang, G.; Kalra, M.K.; Yan, P. Deep learning predicts cardiovascular disease risks from lung cancer screening low dose computed tomography. Nat. Commun. 2021, 12, 2963.

106. Wolterink, J.; Leiner, T.; Takx, R.A.; Viergever, M.; Išgum, I. An Automatic Machine Learning System for Coronary Calcium Scoring in Clinical Non-Contrast Enhanced, ECG-Triggered Cardiac CT; SPIE: San Diego, CA, USA, 2014; Volume 9035.

107. Sandstedt, M.; Henriksson, L.; Janzon, M.; Nyberg, G.; Engvall, J.; De Geer, J.; Alfredsson, J.; Persson, A. Evaluation of an AI-based, automatic coronary artery calcium scoring software. Eur. Radiol. 2020, 30, 1671–1678.

108. Nakanishi, R.; Rajani, R.; Cheng, V.Y.; Gransar, H.; Nakazato, R.; Shmilovich, H.; Otaki, Y.; Hayes, S.W.; Thomson, L.E.; Friedman, J.D.; et al. Increase in epicardial fat volume is associated with greater coronary artery calcification progression in subjects at intermediate risk by coronary calcium score: A serial study using non-contrast cardiac CT. Atherosclerosis 2011, 218, 363–368.

109. Commandeur, F.; Slomka, P.J.; Goeller, M.; Chen, X.; Cadet, S.; Razipour, A.; McElhinney, P.; Gransar, H.; Cantu, S.; Miller, R.J.H.; et al. Machine learning to predict the long-term risk of myocardial infarction and cardiac death based on clinical risk, coronary calcium, and epicardial adipose tissue: A prospective study. Cardiovasc. Res. 2020, 116, 2216–2225.

110. Eisenberg, E.; McElhinney, P.A.; Commandeur, F.; Chen, X.; Cadet, S.; Goeller, M.; Razipour, A.; Gransar, H.; Cantu, S.; Miller, R.J.H.; et al. Deep Learning-Based Quantification of Epicardial Adipose Tissue Volume and Attenuation Predicts Major Adverse Cardiovascular Events in Asymptomatic Subjects. Circ. Cardiovasc. Imaging 2020, 13, e009829.

111. Han, D.; Kolli, K.K.; Gransar, H.; Lee, J.H.; Choi, S.Y.; Chun, E.J.; Han, H.W.; Park, S.H.; Sung, J.; Jung, H.O.; et al. Machine learning based risk prediction model for asymptomatic individuals who underwent coronary artery calcium score: Comparison with traditional risk prediction approaches. J. Cardiovasc. Comput. Tomogr. 2020, 14, 168–176.

112. Tamarappoo, B.K.; Lin, A.; Commandeur, F.; McElhinney, P.A.; Cadet, S.; Goeller, M.; Razipour, A.; Chen, X.; Gransar, H.; Cantu, S.; et al. Machine learning integration of circulating and imaging biomarkers for explainable patient-specific prediction of cardiac events: A prospective study. Atherosclerosis 2021, 318, 76–82.

113. Nakanishi, R.; Slomka, P.J.; Rios, R.; Betancur, J.; Blaha, M.J.; Nasir, K.; Miedema, M.D.; Rumberger, J.A.; Gransar, H.; Shaw, L.J.; et al. Machine Learning Adds to Clinical and CAC Assessments in Predicting 10-Year CHD and CVD Deaths. JACC Cardiovasc. Imaging 2021, 14, 615–625.

114. Antonopoulos, A.S.; Sanna, F.; Sabharwal, N.; Thomas, S.; Oikonomou, E.K.; Herdman, L.; Margaritis, M.; Shirodaria, C.; Kampoli, A.M.; Akoumianakis, I.; et al. Detecting human coronary inflammation by imaging perivascular fat. Sci. Transl. Med. 2017, 9, eaal2658.

115. Oikonomou, E.K.; Marwan, M.; Desai, M.Y.; Mancio, J.; Alashi, A.; Hutt Centeno, E.; Thomas, S.; Herdman, L.; Kotanidis, C.P.; Thomas, K.E.; et al. Non-invasive detection of coronary

inflammation using computed tomography and prediction of residual cardiovascular risk (the CRISP CT study): A post-hoc analysis of prospective outcome data. Lancet 2018, 392, 929–939.

116. Oikonomou Evangelos, K.; Desai Milind, Y.; Marwan, M.; Kotanidis Christos, P.; Antonopoulos Alexios, S.; Schottlander, D.; Channon Keith, M.; Neubauer, S.; Achenbach, S.; Antoniades, C. Perivascular Fat Attenuation Index Stratifies Cardiac Risk Associated with High-Risk Plaques in the CRISP-CT Study. J. Am. Coll. Cardiol. 2020, 76, 755–757.
117. Oikonomou, E.K.; Williams, M.C.; Kotanidis, C.P.; Desai, M.Y.; Marwan, M.; Antonopoulos, A.S.; Thomas, K.E.; Thomas, S.; Akoumianakis, I.; Fan, L.M.; et al. A novel machine learning-derived radiotranscriptomic signature of perivascular fat improves cardiac risk prediction using coronary CT angiography. Eur. Heart J. 2019, 40, 3529–3543.